REPORT DOCUMENTATION PAGE

Form Approved
OMB No. 0704-0188

1. AGENCY USE ONLY (Leave blank)	2. REPORT DATE	3. REPORT TYPE AND DATES COVERED
		FINAL TECHNICAL REPORT 7/1/92-12/31/95

4. TITLE AND SUBTITLE
3-D Optical Memory Disk

5. FUNDING NUMBERS
F49620 92 J 0400
61102F
2305/DS

6. AUTHOR(S)
Demetri Psaltis, Principal Investigator

7. PERFORMING ORGANIZATION NAME(S) AND ADDRESS(ES)
California Institute of Technology
MS 136-93
Pasadena, CA 91125

AFOSR-TR-96
0134

9. SPONSORING/MONITORING AGENCY NAME(S) AND ADDRESS(ES)
AFOSR /NE
Bolling AFB, Washington DC

10. SPONSORING/MONITORING AGENCY REPORT NUMBER
F49620-92-J-0400

11. SUPPLEMENTARY NOTES

19960322 040

12a. DISTRIBUTION/AVAILABILITY STATEMENT
APPROVED FOR PUBLIC RELEASE: DISTRIBUTION UNLIMITED

12b. DISTRIBUTION CODE

13. ABSTRACT

Holographic 3-D disks were investigated and experimentally demonstrated. The storage density of hjolographic disks was theoretically calculated to be in excess of 100 bits per micron squared for media that are approximately 4 mm thick. An experimental demonstration of a system with density equal to 10 bits per micron squared was demonstrated with error free data retrieval in a 100 micron thick photopolymer film. The allignment sensititvity of holographic disks was systematically investigated and it was shown that Fourier/Fresnel plane storage is generally preferrable in this respect. Two new multiplexing methods were developed. The first, peristrophic multiplexing, augments the storage density achievable with angle multiplexing by a factor approximately equal to 4. The second multiplexing method we developed is shift multiplexing in which the rotation of the disk is conveniently used to access multiplexed holograms, making the design of the overall holographic disk system particularly simple.

14. SUBJECT TERMS

15. NUMBER OF PAGES
38

16. PRICE CODE

17. SECURITY CLASSIFICATION OF REPORT	18. SECURITY CLASSIFICATION OF THIS PAGE	19. SECURITY CLASSIFICATION OF ABSTRACT	20. LIMITATION OF ABSTRACT
UNCLASSIFIED	UNCLASSIFIED	UNCLASSIFIED	

AFOSR GRANT NO. F49620 92 J 0400

Final Technical Report

3-D OPTICAL MEMORY DISK

Demetri Psaltis

Submitted to:

Dr. Alan E. Craig
Air Force Office of Scientific Research
Bolling Air Force Base, Washington D.C.

Principal Investigator:

Dr. Demetri Psaltis
California Institute Of Technology
Department of Electrical Engineering
Pasadena, California 91125

Grant AFOSR F 49629-92-J-0400
Final Technical Report
3-D OPTICAL MEMORY DISK

Abstract:

Holographic 3-D disks were investigated and experimentally demonstrated. The storage density of hjolographic disks was theoretically calculated to be in excess of 100 bits per micron squared for media that are approximately 4 mm thick. An experimental demonstration of a system with density equal to 10 bits per micron squared was demonstrated with error free data retrieval in a 100 micron thick photopolymer film. The allignment sensititvity of holographic disks was systematically investigated and it was shown that Fourier/Fresnel plane storage is generally preferrable in this respect. Two new multiplexing methods were developed. The first, peristrophic multiplexing, augments the storage density achievable with angle multiplexing by a factor approximately equal to 4. The second multiplexing method we developed is shift multiplexing in which the rotation of the disk is conveniently used to access multiplexed holograms, making the design of the overall holographic disk system particularly simple.

Optical Memory Disks

The schematic diagram of a holographic 3-D disk system [1,2] is shown in Figure 1. The holographic disk is a photopolymer film laminated on a glass substrate in the shape of a disk. The disk is rotated by a mechanical drive as in a conventional disk system, while the optical head is considerably more complex than the head of a regular CD player. For a read/write system, it consists of a spatial light modulator (SLM), optics, a mechanism for multiplexing holograms, and a 2-D detector array. Any location on the disk can be addressed by the combined mechanical motions of the disk rotation and the translation of the optical head radially. Multiple holograms are overlapped at each location using hologram multiplexing methods such as angle [3,4], wavelength [5,6], phase-code [7,8], fractal [9,10], peristrophic [11], and shift [12] multiplexing. The particular implementation we describe in this report utilizes a combination of angle and peristrophic multiplexing. However most of our conclusions apply to a disk implemented with any multiplexing method.

Data is recorded in the form of 2-D pages presented on the SLM. An optical system transfers the SLM information onto the disk. A hologram is formed by recording the interference between this signal beam and a plane wave reference. The recorded page is read out by illuminating the hologram with the plane wave reference used for recording. The reconstruction is imaged onto the CCD. If the angle of the reconstructing beam is rotated in the plane defined by the wave-vector of the recording reference and the central ray of the signal beam, then the hologram becomes Bragg mismatched due to the finite thickness of the medium and the reconstruction disappears almost completely. Additional

holograms can be recorded and independently retrieved with such rotated references. If the read-out plane wave is rotated around the surface normal, as shown in Figure 1, then for relatively thin media the hologram remains Bragg matched and a reconstruction is produced. However, the rotation of the read-out beam induces a proportional change in the angle of the reconstructed beam. If this angular change is larger than the angular bandwidth of the recorded hologram, it can be blocked by inserting an aperture in the system. A new hologram can then be recorded at this new position of the reference beam. The process is repeated indefinitely until the reference is rotated by 360 degrees. The number of holograms that can be superimposed at one location using the combination of these two multiplexing techniques (angle and peristrophic) is determined by the thickness of the medium and the bandwidth of the signal beam.

Holograms in the holographic 3-D disk can be recorded in the image, Fourier, or Fresnel planes. Selection of one method over another is primarily based on the available optics, spatial light modulators, detector arrays, quality of the resulting holograms, complexity of the setup, and surface density. In order to maximize the surface density of a holographic 3-D disk, it is necessary to pack as many bits into as small a surface as possible. Therefore, for image plane holograms, each pixel (bit) must be as small as possible. On the other hand, to achieve high surface density with Fourier plane holograms, it is better to have large pixels so that the Fourier transform is small (Fourier transform of a square pixel produces a spot size in 1-dimension equal to $2\lambda F/\delta$, where λ is the wavelength, F is focal length, and δ is the pixel size). While there are expensive stepper lenses that can produce large images with pixels less than a micron in size, it is generally easier to obtain lenses that resolve larger pixels. Furthermore, image plane

holography generally requires more lenses than Fourier plane to relay the image unto the recording material and then to the read-out detector array. One disadvantage of recording Fourier transformed holograms is that the intensity of the signal beam is usually very non-uniform. Consequently, the quality of the reconstructed hologram is poor due to the strong DC present during recording. One way to get around this problem is by using a pixel-to-pixel matched phase diffuser right after the SLM. This way, the signal beam will be approximately uniformly distributed in the Fourier plane while the size of the recording spot does not increase. Another method to fix this problem is by recording the hologram slightly off of the exact Fourier plane (Fresnel plane). In the Fresnel plane, the intensity is more evenly distributed at the cost of a slightly larger spot size. We used Fresnel plane recording in our experiments.

The most important performance characteristics of holographic 3-D disks are the surface density, recording characteristics (rate and linearity), the read-out rate, and the signal-to-noise ratio (SNR) of the reconstructions. We assembled an experimental apparatus with which we evaluated these performance characteristics for a holographic disk implemented with 100 μm thick Dupont photopolymer. A diagram of the experimental set-up is shown in Figure 2. A glass plate of a random binary bit pattern was used as the input SLM. The center-to-center spacing of the pixels was 45 microns and the fill factor was 100%. Nikon F/1.4, 3.9 cm aperture camera lenses were used for imaging (the glass mask plate was pressed up against the Nikon lens to ensure all the pixels within the lens aperture were captured). A total of 590,000 pixels fit in the apertures of the two Nikon lenses and a sharp image of the entire field was obtained at the CCD plane. The holograms were recorded with a plane reference beam approximately .5 mm past the

Fourier transform plane. At that position, the diameter of the signal beam was 1.5 mm and its spatial uniformity was much better than at the exact Fourier plane. For simplicity, peristrophic multiplexing was achieved by rotating the recording material, instead of the reference beam, around the surface normal. Angle multiplexing was combined with peristrophic multiplexing to increase the number of pages stored at each location.

In the remainder of the report, we report a sequence of experimental results from this apparatus that give us a good estimate for the performance we can expect from a polymer-based holographic disk. Specifically, in section II we derive the surface density realizable with the 100 μm thick film. In section III we describe the recording characteristics of the polymer which yield the linearity and the recording rate of the system. In section IV we measure the diffraction efficiency of the holograms and thus determine the achievable read-out rate while in section V, we report our measurements of the fidelity of the reconstructions and show that density of at least 10 bits/μm^2 can be achieved with low probability of error. Finally, we summarize the results and conclude in section VI.

II. Surface Density

The surface density of current compact disk memories is approximately 1 bit/μm^2 and it is primarily limited by the size of the illuminating spot. The new generation of optical CDs that are scheduled to appear in the near future will likely have storage density around 5 bits/μm^2 [13] per layer. Dual layer and double-sided systems are expected to have equivalent storage density in excess of 10 bits/μm^2. In order for holographic memories to be competitive, the density of holographic disks must be higher than the projected density of conventional media by a comfortable margin. This concern makes

storage density the primary goal in the design of a holographic disk. The storage density of holographic disks was analyzed by Li and Psaltis [2] who showed that for the optimum thickness of the recording medium (L = 1.6 cm), we can obtain a density of 110 bits/μm^2 using angle multiplexing. This gives more than an order of magnitude margin over the projected 5 bits/μm^2 of conventional CD technology. The method we present in this report can achieve higher densities than those predicted in [2] for relatively thin recording media such as the photopolymer.

To a first approximation, the density of a holographic disk is given by :

$$D_{3D} = M \times D_{2D} \tag{1}$$

where D_{3D} and D_{2D} are the surface densities achievable with a 3-D and 2-D medium, respectively, and M is the number of holograms multiplexed. The density predicted by Equation (1) is a theoretical upper limit that can be difficult to achieve in practice. For example, Equation (1) holds only if the resolution of the conventional CD lens and the lens in the signal arm of the system in Figure 2 are the same. This is possible but difficult since the 3-D memory must maintain the same resolution over a large field whereas the CD lens only needs to produce a single spot at the optical axis of the lens. The recording medium's dynamic range can also limit the storage density since the diffraction efficiency falls off as $1/M^2$. Finally, some noise sources such as cross-talk increase as M gets larger. In a practical system, the storage density is maximized by optimizing the optical design while monitoring the signal-to-noise ratio of the reconstructed holograms.

The maximum number of holograms that can be angularly multiplexed at each location is given by :

$$M_{angle} = \frac{\Theta}{\Delta\theta} = \frac{\Theta L \sin(\theta_r + \theta_s)}{\lambda \cos(\theta_s)} \qquad (2)$$

where Θ is the range of angles that can pass through the aperture of the optical system in the reference arm, $\Delta\theta$ is the angular selectivity, L is the thickness of the hologram, λ is the wavelength of the laser, θ_r (θ_s) is the angle between the reference (signal) beam and the disk surface normal (in this report, all parameters are referenced to inside the recording material). We can obtain an expression for the 3-D storage density by substituting Equation (2) into Equation (1). If we assume that D_{2D} is independent of L (reasonable for relatively thin media) then we obtain $D_{3D} \sim L$. In Figure 3 we plot the surface density as a function of L calculated using the analysis of reference [2] and also Equations (1) and (2) from this report. We see that the approximate analysis yields a density estimate that is very close to the estimate of the detailed analysis for thickness up to 100 μm. Therefore we will use Equation (1) to calculate the density of a disk that is implemented with the 100 μm thick polymer.

For our experimental setup, L = 100 μm, λ = 349 nm (532 nm outside), θ_r = 22°, and θ_s = 16°, which gives $\Delta\theta$ a value of .31° to the first null of the sinc function (the index of refraction for Dupont's photopolymer is 1.525). However, Equation (2) is only valid for plane wave holograms. The signal beam spread inside was nearly 26 degrees due to the large numerical aperture of the F/1.4 Nikon lenses. When 3 holograms were angularly multiplexed, the SNR measured was 4 and 3.2 for an angular separation of 3.3° and 1.3°, respectively, while the SNR measured for a single recorded hologram was 4.5. Therefore, we selected to angularly separate the holograms by 1.6° (2.5° outside angle) to strike a balance between density and cross-talk noise. Consequently, with $\Delta\theta$ = 1.6° and a

geometrically limited Θ of approximately 14°, up to 8 holograms can be angularly multiplexed at a given location. Since the photopolymer has enough dynamic range to record more than 8 holograms, we introduce peristrophic multiplexing to increase the storage density.

As shown in Figure 1, peristrophic multiplexing is achieved by rotating the reference beam around the film's surface normal after each hologram is recorded (or by rotating the film around the reference beam). The rotation causes the reconstruction to exit at a different direction where it can be filtered, allowing a new hologram to be stored and retrieved without cross-talk. The change in peristrophic angle required to move the reconstruction off the detector is independent of L. For Fourier plane holograms, the amount of rotation required to shift the reconstructed image off of the detector array is [11]:

$$\Delta\psi_{Fourier} = \frac{\frac{d}{F}}{\sin\theta_r + \sin\theta_s} \tag{3}$$

where d is the size of the reconstructed image in the detector plane and F is the focal length of the lens used. For image plane holograms, the amount of rotation required to filter out the undesired reconstruction in the Fourier plane of the system with a spatial filter is:

$$\Delta\psi_{Image} = \frac{\frac{2\lambda}{\delta}}{\sin\theta_s + \sin\theta_r} \tag{4}$$

where $1/\delta$ is the highest spatial frequency in the image. Peristrophic multiplexing in either the image or Fourier planes gives essentially no cross-talk between the recorded

holograms. This is due to the fact that the undesired holograms are blocked and do not interfere with the desired hologram.

When $\theta_r = \theta_s$, it is possible to multiplex peristrophic holograms in the range between 0 and π before degeneracy occurs. If the signal is perpendicular to the film surface ($\theta_s = 0$) and θ_r is large enough, then it is possible to multiplex peristrophic holograms from 0 to 2π. For example, if the goal is to store many holograms in the same location without regards to density, we can choose d = 1 cm, F = 50 cm, δ = 50 μm, L = 100 μm, λ = 349 nm, $\theta_r = 30°$, and $\theta_s = 0°$. Then $\Delta\psi_{Fourier} = 2.3°$, and $\Delta\psi_{Image} = 1.6°$. Therefore, up to 225 holograms can be recorded using peristrophic multiplexing in the image plane. On the other hand, if the surface density is important, then we might chose d = 3.9 cm, F = 5.5 cm, δ = 1 μm, L = 100 μm, λ = 349 nm, $\theta_r = 22°$, and $\theta_s = 16°$ (the exact setup used in our experiment, except for δ). Then $\Delta\psi_{Fourier} = 63°$, and $\Delta\psi_{Image} = 61.5°$. In this case, only up to two peristrophic holograms can be recorded. In our setup, the recording material was tilted an additional 5° in the plane perpendicular to the plane formed by the reference and signal beams to enhance the effects of peristrophic rotation on shifting the spectrum off of the κ-sphere. Experimentally, we found that in this tilted configuration, 45° in rotation was sufficient to completely Bragg-mismatch and shift the undesired hologram off of the detector array. Therefore, up to four peristrophic holograms can be multiplexed from 0 to π using this configuration. Sets of 8 angularly multiplexed holograms were recorded at each of the 4 different peristrophic positions. Angle multiplexing was achieved by rotating the film in the plane formed by the signal and reference beam instead of changing the reference beam angle. Using this method, we

stored a total of $M = 8 \times 4 = 32$ holograms at a single location. A window from one of the 32 reconstructions is shown in Figure 4.

Having determined M we now need to calculate D_{2D} in order to find the density of the 3-D disk. D_{2D} is computed by dividing the total number of SLM pixels that are holographically recorded (590,000) by the area occupied by the signal beam on the medium ($\pi \times .75 \times .75$ mm^2). Using this definition, we obtain $D_{2D} = 0.334$ bits/μm^2. Since 32 holograms are superimposed in the same location, the overall surface density is $32 \times .334 = 10.68$ bits/μm^2. We can further improve the density of the current system by using lower F/# lenses (higher resolution and density per page), reducing the angular separation between holograms, and increase the range of angles over which angle holograms can be recorded. The density can of course be increased by a large factor (see Figure 3) if a thicker recording medium is used. The small thickness is the most serious shortcoming of the Dupont polymer for the 3-D disk application.

III. Recording Rate and Linearity

The rate at which data can be recorded on the holographic disk, without taking into account the over-head of multiplexing, is :

$$R_{in} = \frac{N_p}{\tau_{in}} \tag{5}$$

where N_p is the number of pixels per page and τ_{in} is the time required to record one hologram.

The recording time, τ_{in}, is determined by the sensitivity of the recording medium and the desired diffraction efficiency per hologram. For Dupont's 100 micron thick photopolymer (HRF-150), the diffraction efficiency as a function of exposure energy is

shown in Figure 5. Figure 5 was obtained by integrating the diffraction efficiencies of 50 plane wave peristrophic holograms, each exposed to 7 mJ/cm^2 with λ = 320 nm (488 nm outside) and $\theta_r = \theta_s = 19.2°$. This particular recording material is fairly insensitive until it is exposed by about 35 mJ/cm^2. It then exhibits a quasi-linear recording behavior and flattens out as the material nears saturation around 325 mJ/cm^2. This means that the holograms recorded later in the sequence require a longer exposure time to achieve the same diffraction efficiency as the earlier holograms. We use a recording schedule that compensates for the lost of grating strength as the material saturates, thereby using all the available dynamic range of the material.

The recording schedule is derived by taking the square-root of Figure 5 to obtain the hologram grating strength as a function of exposure energy. This curve is then modeled by fitting it to a 6th order polynomial, *F(E)*. By taking the derivative of the polynomial with respect to exposure energy, the local grating growth rate, $f(E) = F'(E)$ (in units of cm^2/Joule), as a function of exposure energy is obtained. Given *f(E)*, the strength of each hologram to be multiplexed can be pre-determined by allocating the exposure energy appropriately. Specifically, equal strength holograms can be recorded by allocating the entire dynamic range of the photopolymer equally among the holograms. The desired exposure for the nth hologram to achieve equal diffraction efficiencies for all the holograms is:

$$t_n = \frac{A_{sat}}{Mf(E_{n-1})I} \tag{6}$$

where t_n is the exposure time for the nth hologram, A_{sat} is the saturation grating strength, M is the number of holograms, E_{n-1} is the cumulative exposure energy up to the n-1th

hologram, and I is the exposure intensity. We pre-expose the material with 35 mJ/cm^2 worth of energy (E_0 = 35 mJ/cm^2) to make it sensitive before recording any holograms.

An exposure schedule for 50 holograms was calculated using Equation (6) and Figure 6 shows the result. Notice that the exposure time per hologram increases as the film becomes more saturated. The diffraction efficiencies of the 50 holograms that were recorded with the schedule shown in Figure 6 were more uniform than when equal exposure time were used, but still not equal. This is due to the fact that the scheduled exposure time changes the overall exposure the film receives before the nth exposure, compared to the equal exposure schedule with which Figure 5 was calculated. This run-time effect [14] is taken into account by iterating the previous procedure of integrating the square-root of the diffracted power from the 50 newly recorded holograms, fitting the new curve to the polynomial, and then generating a new schedule using Equation (6). An interesting by-product of this recording procedure is that the saturation grating strength, A_{sat}, increases by a few percent for the scheduled recording. Figure 7 shows the diffraction efficiency of the 50 holograms that were recorded using two iterations of the recording schedule. From Figure 7 it can be seen that the diffraction efficiency is uniformly distributed among the 50 holograms. The above iterative procedure can be repeated until the desired uniformity is reached.

By using the recording schedule, the recording time is different for each page of data and therefore, the recording rate also changes. If a buffer is used to store all the holograms that are to be recorded at one location, then the appropriate measure is the average recording rate:

$$\overline{R}_{in} = \frac{MN_P}{\sum_{n=1}^{M} \tau_{in}(n)} = \frac{M^2 N_P I}{A_{sat} \sum_{n=1}^{M} \frac{1}{f(E_{n-1})}} \qquad (7)$$

From the parameters of our experimental set-up, we predict from Equation (7) a recording rate of 130 Kbits/sec. In the high density experiment however, we were not able to use the recording schedule procedure as described above. This is because the intensity of the reference beam inside the material varied by ~ 10 percent as its angle was changed by 13° due to the Fresnel reflections from the film surface. This variation in intensity leads to additional non-uniformity in the recorded holograms. These variations can in principle be eliminated by AR coating or compensation of the reference beam amplitude. They can also be removed by continued iterations of our basic exposure schedule procedure using a higher order polynomial to model the curve that describes the dependence of the cumulative grating strength on the exposure. Instead, we were able to obtain the recording schedule for equalizing the 32 holograms simply through trial and error.

In selecting the exposure time we are faced with the trade-off between diffraction efficiency and quality of the reconstructions. Clearly, if the entire dynamic range of the recording material is used, then the diffraction efficiency of each of the equalized holograms is maximized. On the other hand, the quality of the reconstructions degrades when the entire dynamic range is used. This degradation occurred when we attempted to record high density data in the Fresnel plane. We believe this effect is due to the index modulation in the recording area from the multiple exposures, (or equivalently inter-pixel gratings), that distort the images traveling through the medium. In order to minimize this

effect we restricted the recording to only around 30 percent of the dynamic range of the medium.

A recording rate of .7 Mbits/s was experimentally demonstrated in the high density set-up. This was done by recording 590,000 pixel holograms in an average recording time of 840 ms per hologram. The total incident intensity was 2 mW/cm^2 and the diffraction efficiency per hologram was ~ .35%. From Equation (7) and our experimental observations with plane wave holograms, we know that the recording time for achieving the same diffraction efficiency is approximately inversely proportional to the incident intensity for intensities greater than 2 mW/cm^2. For intensities less than 2 mW/cm^2, the diffraction efficiency drops as the recording intensity is increased while the total exposure energy remains the same due to the diffusion limited process inherent in this material [15]. Therefore, if the total incident intensity is increased from 2 mW/cm^2 to 128 mW/cm^2, then the average recording time per hologram drops to 13 ms and the recording rate becomes 45 Mbits/s. Notice that the recording rate we obtained experimentally (.7 Mbits/sec) is substantially faster than the rate predicted by Equation (7) (130 Kbits/sec). This is because we only used a small, linear portion of the material's dynamic range in the experiment.

IV. Read-out Rate

One of the limiting factors for the read-out-rate is the time, τ, it takes to accumulate sufficient number of photons per CCD pixel so that the reconstructions can be reliably detected above the noise floor. We can estimate τ as follows

$$\tau = \frac{PhcN_p}{\eta I_{inc} \lambda_{outside}} \qquad (8)$$

where P is the minimum number of photons per pixel, h is the Planck's constant, c is the speed of light, N_p is the total number of pixels, η is the diffraction efficiency, I_{inc} is the incident power of the read-out beam, and $\lambda_{outside}$ is the wavelength outside of the material. We will use a generous choice of P = 1,000 photons for the calculation. The rest of the parameters in Equation (8) have already been determined in our experimental set-up except for the hologram diffraction efficiency η. If we multiplex M holograms in a linear, saturable material using the full dynamic range of the material, then the amplitude of each recorded hologram becomes [16] $R^*S \propto A_{sat}/M$. Since diffraction efficiency is proportional to the grating strength squared, the diffraction efficiency can be written as:

$$\eta = \left(\frac{M/\#}{M}\right)^2 \tag{9}$$

where the quantity $M/\#$ characterizes the efficiency of the material in the recording geometry that it is being used. Since we have already determined that M = 32, we can determine η by measuring the $M/\#$. We recorded in the HRF-150-38 (product number of the 38 μm Dupont polymer) sets of 10, 25, 50, 75 and, 90 plane wave holograms using peristrophic multiplexing and the recording schedule previously described. The same procedure was performed for the HRF-150-100 (the 100 μm thick polymer) with sets of 25, 50, 75 and 90 plane wave holograms. The resulting diffraction efficiencies are plotted in Figure 8 as a function of the number of holograms. We can see that the experimental data agrees very well with the $1/M^2$ theoretical prediction. The $M/\#$ measured from Figure 8 is $M/2.2$ and $M/6.5$ for the 38 μm and 100 μm thick films, respectively.

If we want to store 1,000 holograms in the HRF-150-100 photopolymer using the same setup used to measure the $M/\#$ (λ = 320 nm and $\theta_r = \theta_s$ = 19.2°) then Equation (9)

predicts a diffraction efficiency per hologram of approximately $\eta = 4 \times 10^{-5}$. We verified this experimentally by storing 1,000 image plane holograms of a random binary mask using a combination of peristrophic and angle multiplexing (100 peristrophic holograms at each of the 10 angular locations). The surface density in this case was much lower than 10 bits/μm^2 because of the large pixels used. Figure 9 shows the diffraction efficiency as a function of hologram number for the 1,000 hologram experiment (the diffraction efficiency was corrected for the half-on, half-off nature of the binary mask). The result of Figure 9 was obtained after six iterations through the recording schedule procedure. The sharp non-uniformities are attributed to stage instability during recording. A reconstruction of one of the 1,000 stored holograms in shown in Figure 10. Figure 11 shows the cross-section through the same reconstruction. The quality of the reconstructions is excellent.

Using the experimentally measured *M*/6.5 for the HRF-150-100 photopolymer film, the diffraction efficiency per hologram for the high density experiment (32 holograms) should be about 4×10^{-2} for each hologram. However, the experimentally measured diffraction efficiency was $\eta = 3.5\times10^{-3}$. This is attributed to the fact that we only used 30% of the dynamic range of the material which effectively reduces A_{sat} to less than one-third of its value. The diffraction efficiency then drops by the square of this reduction. If we use the actual parameters of our experiment, N_p = 590,000, $\eta = 3.5\times10^{-3}$, I_{inc} = 1 mW, and $\lambda_{outside}$ = 532 nm, then the required integration time becomes approximately $\tau = 65$ μs. The expression for the read-out rate, R_{out}, is simply:

$$R_{out} = \frac{N_p}{\tau_{out}} \tag{10}$$

where N_p is the number of pixels per hologram and τ_{out} is the time required to read each hologram. For $\tau = \tau_{out} = 65$ μs, $R_{out} = 9$ Gbits/sec using $N_P = 590{,}000$ pixels. This read-out rate was not actually realized in the experimental set-up because the CCD we used cannot read an entire page of data in 65 μs and it does not have enough resolution to read all 590,000 pixels. The CCD read-out windows of 65 × 65 pixels at video rate resulting in the much more modest read-out rate of .13 Mbits/s actually demonstrated in our high density experiment setup. If a large, parallel read-out CCD detector array is used to read out the entire 590,000 pixels in a minimum frame-transfer-rate of 1000 frames/s, then a detector limited read-out rate greater than 500 Mbits/s can be achieved.

The motion of the disk introduces an additional constraint in the selection of the integration time on the detector. The motion of the disk causes the reconstructed image on the CCD to also move. If the integration time is too long then the motion of the reconstruction causes smearing. Li and Psaltis [17] derived the maximum allowable dwell time on the CCD to be ~ 2.7 μs, using a disk rotation rate of 3600 RPM. Therefore, in a continuously spinning disk system, the minimum required integration time cannot be as long as the 65 μs of the current experimental set-up. The integration time can be lowered by a factor of 65 to approximately 1 μs by increasing the laser power and/or increasing the diffraction efficiency of the hologram. We can accomplish the same thing by decreasing the number of pixels per page. However the optical system would have to be redesigned to sustain the same surface density. Also the recording rate goes down if the number of pixels per page is reduced, but this is not important if the application is a read-only memory. For example, if we use $N_p = 300{,}000$, $\eta = 4\times10^{-2}$, $I_{inc} = 60$ mW, and $\lambda_{outside} =$ 500 nm, then the required integration time per pixel is only ~ 50 ns. The laser source

could be pulsed for 50 ns to freeze the reconstruction on the detector and thus avoid smearing while the CCD reads out the detected image. In this case, the read-out rate again becomes limited by the frame transfer rate of the CCD camera.

V. Reconstruction Fidelity

The most challenging aspect of the high density experiment proved to be the suppression of noise in the system in order to achieve acceptable levels of SNR and probability of error. We reported earlier in this report the storage of 1,000 holograms in the Dupont photopolymer. We were able to retrieve all the bits in the 1,000 stored holograms with very low probability of error (no errors were actually detected in the bits that were tested). Since the high density experiment requires only 32 holograms to be stored in order to achieve the goal of 10 bits/μm^2, it may seem simple to demonstrate low probability error for this experiment. In fact, this was not the case. The way we achieve high density is by increasing the angular bandwidth of the signal and reference arms. The noise level goes up as the angular bandwidth increases for the majority of noise sources, while the signal level does not. Consequently, the SNR starts to decrease as we attempt to achieve higher surface density and it becomes necessary to carefully track each of the noise sources and optimize the system in order to minimize their effect. Through this process we were able to demonstrate storage at 10 bits/μm^2 with SNR = 3.5 without any errors detected among the bits that were tested. In the remainder of this section we will discuss the noise sources in the system and we will describe the steps we took to minimize them.

We can divide the noise sources into two categories: system noise and hologram noise. Lens aberrations, SLM imperfections, detector noise, scattering and multiple

reflections from lenses and other optical components, laser non-uniformity and fluctuations, and SLM to CCD pixel misalignment are examples of system noise. The rest of the noise arises from the hologram itself. Specifically, the hologram can introduce cross-talk between the recorded holograms, inter-pixel cross-talk, scattering from the recording material, multiple reflections in the medium, non-uniform diffraction efficiency in the recorded holograms, distortions due to surface imperfections, blurring due to limited spatial resolution of the material and material shrinkage. We can separately determine the system noise level by simply imaging a page of data presented by the SLM onto the CCD and measuring the SNR of the detected image. After we minimize the system noise, holograms are then recorded with the system and we follow a step-by-step procedure to identify the various sources of hologram noise. We use the following definition of SNR to make a comparative assessment of system performance:

$$SNR = \frac{m_2 - m_1}{\sqrt{\sigma_1^{\,2} + \sigma_2^{\,2}}} \tag{11}$$

In the above equation m_1 and σ_1 are the mean and standard deviation of the intensity of the dark pixels, while m_2 and σ_2 are the mean and standard deviation for the white pixels. Since the pixel pitch of the SLM is 45 μm and the pixel pitch of the CCD array is 10 μm, each SLM pixel becomes over-sampled by the CCD pixels with the unit magnification imaging system. The CCD detects a window of 65 × 65 SLM pixels at a time. The video from the CCD is digitized and a computer program automatically outlines the SLM pixels in the image. On the average, each SLM pixel is sampled by 20.5 CCD pixels and the program produces an estimate for the intensity of an SLM pixel by averaging 9.5 CCD pixel values. Therefore, on the average, 11 CCD pixels are discarded as edge pixels when

a measurement of an SLM pixel value is made. The data is then processed to compute the mean and variances so that the SNR in Equation (11) can be calculated. In addition, a histogram of the data is made and the data is classified. These measurements provide estimates for the probability of error.

The SNR obtained for various experimental conditions is plotted in Figure 12. The first measurement is SNR = 10 due to system noise only. This was obtained by transmitting the signal beam through the system without any recording material. The histograms of the dark and white pixels are well separated and no errors were observed. Next, a glass substrate on which the photopolymer is usually laminated on is placed at the recording plane of the system. The SNR drops to 9 due to the slight aberrations caused by the substrate. When we introduced a piece of UV cured photopolymer laminated on a glass substrate at the place where the holograms are normally located, the SNR drops from the upper limit of 9 to around 7. The major cause of this drop in SNR is most likely due to internal reflections within the film and glass substrate and possibly scattering. The interference fringes can be eliminated with anti-reflection coatings applied to both the glass and photopolymer.

A SNR of approximately 4.5 was obtained when a single hologram was recorded and its reconstruction was evaluated. The histograms of the dark and white pixels were still clearly separated and no errors were observed. This shows that the resolution of the photopolymer is sufficient to record high density holograms with clarity. The reason the SNR drops from 7 to 4.5 for one hologram is strongly connected to the internal reflections from the boundaries. As stated before, the signal beam creates an interference pattern (fringes) when it passes through the film and glass substrate. This is also true for the

reference beam when it is brought in to record a hologram. Furthermore, when the reference beam is used to reconstruct the stored holograms, it also creates an interference pattern that can be seen with the naked eye on the film. Therefore, the reconstruction suffers from the fringes that is on the reference beam twice. Other effects such as the fidelity of the recording material also plays a role in degrading the SNR.

The average SNR of three peristrophically multiplexed holograms (60° separation) remains around 4.5. This indicates two things: peristrophic multiplexing does not introduce cross-talk (as expected) and the superposition of 3 holograms does not significantly deteriorate the quality of each hologram. The average SNR of three angle multiplexed holograms (5° outside separation) drops to around 4. This is a clear indication of cross-talk noise in the angle holograms. The SNR further drops to about 3.2 for angle holograms separated by 2° outside angle. With a SNR of only 3.2, the histograms of the dark and white pixels almost overlap but no errors were observed. Based on these measurements, we selected 2.5° (outside) for the angular separation in the angle multiplexing portion of the system.

Inherent to the photopolymer material, there is a shrinkage effect that slightly smears the reconstruction. Furthermore, the shrinkage effect also makes it difficult to Bragg match the entire hologram for read-out. For images with low bandwidth, the shrinkage effect is barely noticeable in both hologram quality and Bragg condition of the entire page. However, in our high density experiment, the bandwidth of the signal beam alone was 26° inside the material. This means when a hologram is reconstructed, only about 1/3 of the page is Bragg matched at a time. The entire page can be viewed by changing the angle of the reference beam slightly (or by rotating the stage that does angle

multiplexing). A simple calculation using experimental observations reveals that the shrinkage in the HRF-150-100 photopolymer film is about 3%. Not being able to see the entire reconstruction at one time could add substantial complexity to the read-out system.

Even with all the noise sources discussed above, we sampled 9 different 65 × 65 pixel windows from the optimized 32 holograms and no errors were detected. The combined histogram from the 9 different sampled windows is shown in Figure 12. Their average SNR is about 3.5. The SNR dropped from 4 (obtained when we angle multiplexed 3 holograms separated by 5°) to 3.5 because the cross-talk noise level increased and inter-pixel gratings started forming due to the 32 exposures. The diffraction efficiency of each hologram was $\eta = 3.5 \times 10^{-3}$ while the equivalent diffraction efficiency of the light scattered from the polymer when it is illuminated by the reference is only 3×10^{-5}. Therefore, scattering is a negligible contributor to the overall noise level. It is likely that there were no errors in any of the 32 stored holograms even though we did not check all the stored bits. An estimate for the probability of error was obtained by fitting a first-order χ^2 distribution to the histogram of Figure 13. The estimated probability of error from this model is approximately 10^{-4}.

VI. Conclusion

We experimentally demonstrated a surface density of 10 bits/μm^2 in the 100 μm Dupont polymer by superimposing 32 holograms, each having a surface density of .334 bits/μm^2. It might be possible to increase the density further by a factor of 2 to 3 by increasing the N.A. of the lenses in the system and possibly reducing the angular separation of the reference beams used for angle multiplexing. However, pressing for substantially higher density in the 100 μm film will be difficult. What is really needed is a

photopolymer with 1 mm thickness which would yield density in the range of 100 bits/μm^2. The recording rate in the experimental set-up was .7 Mbits/s and we extrapolate that 45 Mbits/s is possible if we use incident intensity 128 mW/cm^2. The read-out rate of the experimental set-up was .13 Mbits/s (limited by the CCD detector) and we project that a read-out rate equal to 500 Mbits/s can be achieved with a CCD that has at least 590,000 pixels and reads out 1,000 frames per second. However, the shrinkage of the polymer remains a serious concern that currently complicates the read-out process. No errors were detected in the 38,000 bits that were selected from the 32 reconstructions and evaluated. A theoretical estimate of the expected raw probability of error based on modeling the histogram of the data is approximately 10^{-4}.

VII. Acknowledgment

We gratefully acknowledge the Air Force Office of Scientific Research for sponsoring this research project. We also thank George Barbastathis, Kevin Curtis, and Sidney Li for many helpful discussions.

References

[1] D. Psaltis, "Parallel optical memories." Byte, **17**(9), pg 179-182 (1992).

[2] H.-Y. S. Li and D. Psaltis. "Three dimensional holographic disks." Appl. Opt. **33**(17), pg 3764-3774 (1994).

[3] D. L. Staebler, J. J. Amodei and W. Philips. "Multiple storage of thick holograms in $LiNbO_3$." VII International Quantum Electronics conference, Montreal (1972), pg 611.

[4] F. H. Mok, M. c. Tackitt and H. M. Stoll. "Storage of 500 high-resolution holograms in a $LiNbO_3$ crystal." Opt. Lett. **16**(8) pg 504-607 (1991).

[5] S. Yin, H. Zhou, F. Zhao, M. Wen, Y. Zang, J. Zhang and F. T. S. Yu. "Wavelength-multiplexed holographic storage in a sensitive photorefractive crystal using a visible-light." Opt. Comm. **101**(5-6) pg 171-176 (1991).

[6] G. A. Rakuljic, V. Levya and A. Yariv. "Optical data storage by using orthogonal wavelength-multiplexed volume holograms." Opt. Lett. **17**(2) pg 1471-1473 (1992).

[7] C. Denz, G. Pauliat and F. Roosen. "Volume hologram multiplexing using a deterministic phase encoding method." Opt. Comm. **85** pg 171-176 (1991).

[8] Yoshinao Taketomi, Joseph E. Ford, Hironori Sasaki, Jian Ma, Yeshaiahu Fainman, and Sing H. Lee. "Incremental recording for photorefractive hologram multiplexing." Opt. Lett. **16**(22) pg 1774-1776 (1991).

[9] D. Psaltis, D. Brady, X. G. Gu and S. Lin. "Holography in artificial neural networks." Nature. **343**(6256) pg 325-330 (1990).

[10] F. H. Mok. "Angle-multiplexed storage of 5000 holograms in lithium niobate." Opt. Lett. **18**(11) pg 915-917 (1993).

[11] K. Curtis, A. Pu, and D. Psaltis, Opt. Lett. **19**(13) pg 993-994 (1994).

[12] D. Psaltis, M. Levene, A. Pu, G. Barbastathis, and K. Curtis, "Holographic storage using shift multiplexing," Opt. Lett. **20**(7), pg 782-784 (1995).

[13] Toshiba SD (Super Density) format technical specification.

[14] K. Curtis, and D. Psaltis. "Characterization of the DuPont photopolymer for 3-dimensional holographic storage." Appl. Opt. **33**(23), pg 5396-5399 (1994).

[15] G. Zhao and P. Mouroulis. "Diffusion model of hologram formation in dry photopolymer materials." Journal of Modern Opt. **41**(10) pg 1929-1939 (1994).

[16] D. Brady and D. Psaltis. "Control of volume holograms." Journal of the Optical Society of America. **9**(7) pg 1167-1182 (1992).

[17] H.-Y. S. Li and D. Psaltis. "Alignment sensitivity of holographic three-dimensional disk." *JOSA* A. v12 (**9**), pg 1902-1912 (1995).

List of Figures

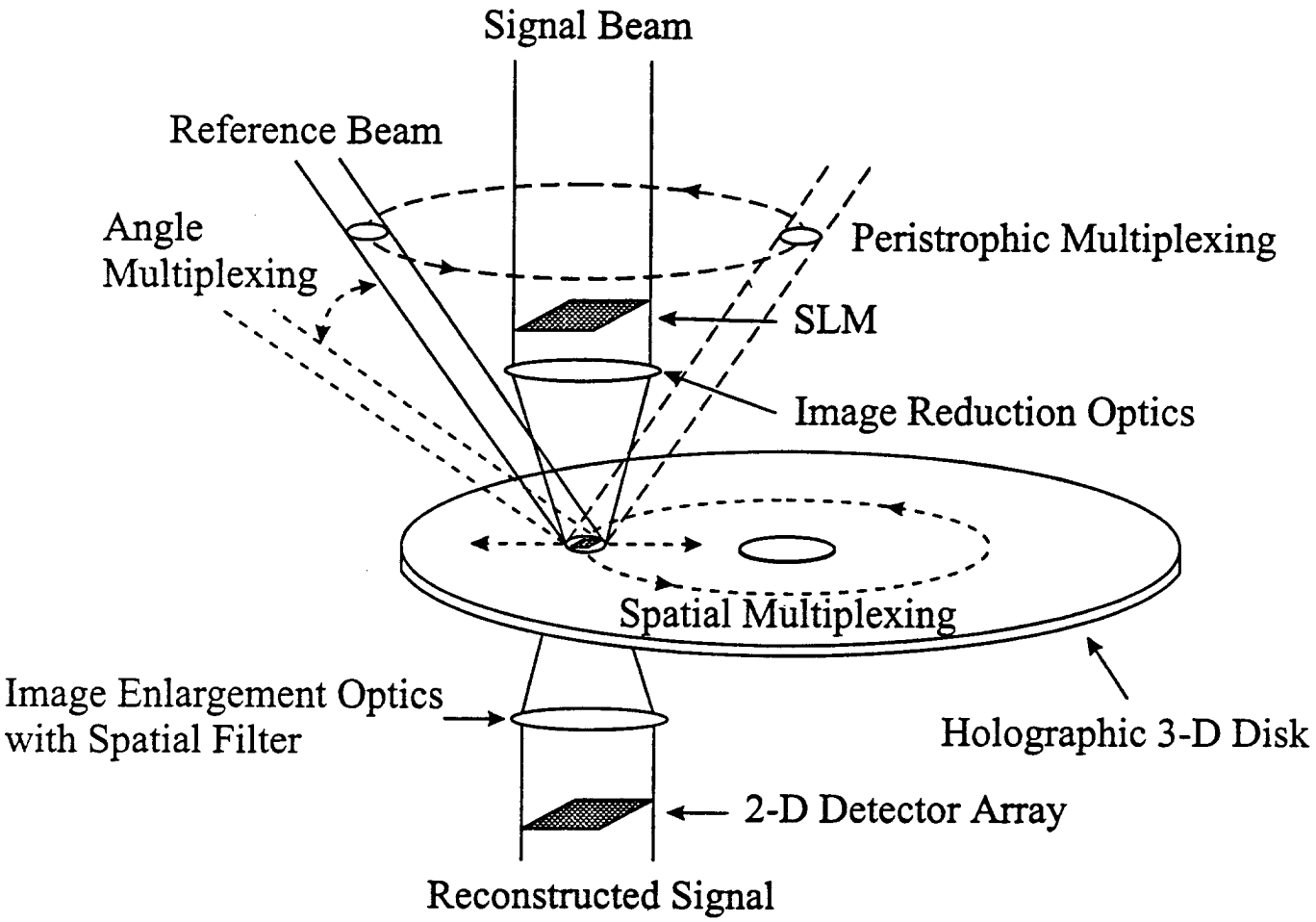

FIG 7 HDAOPA01.CDR

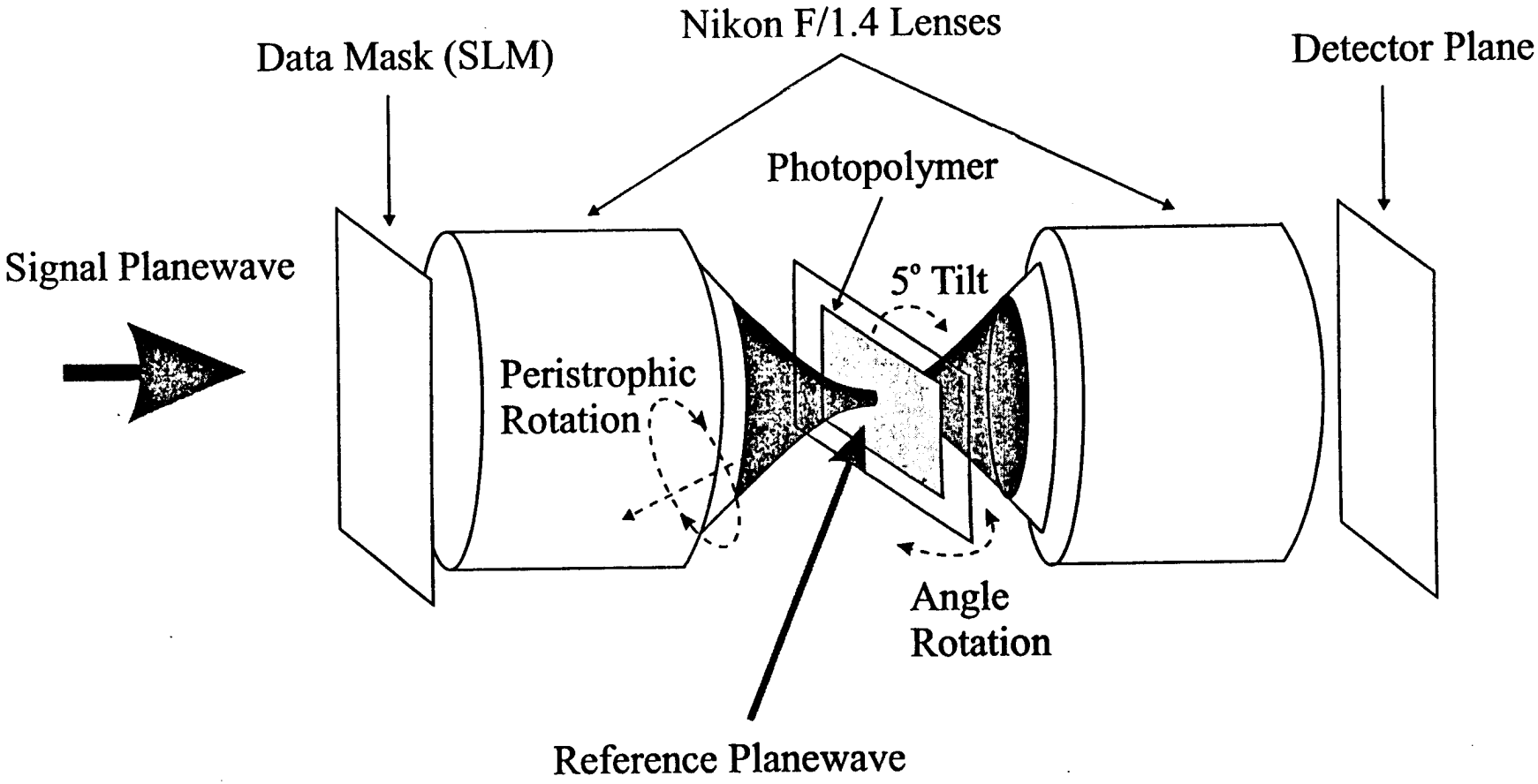

FIG. 2 HDA OPA Ø2 CON2

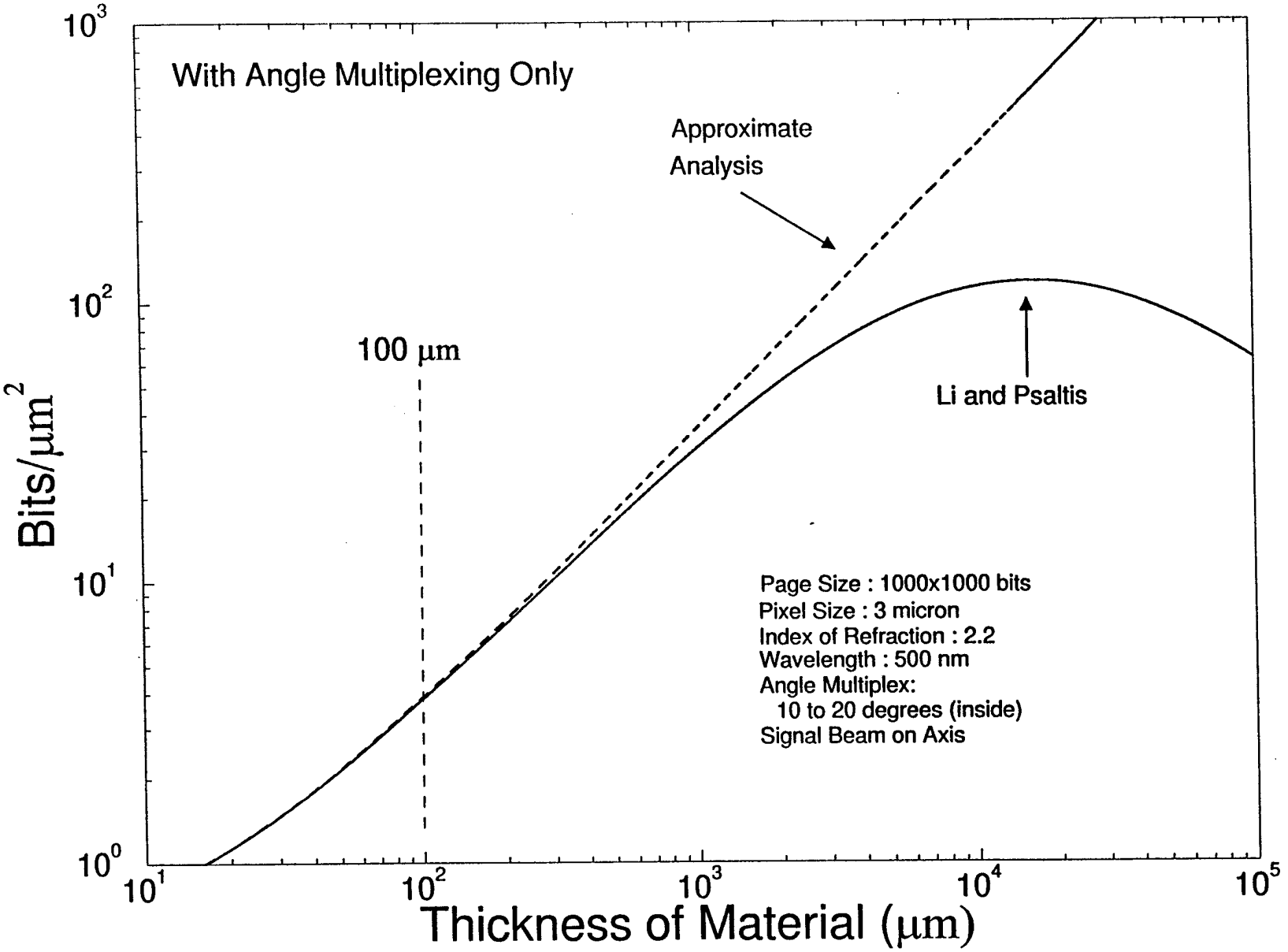
With Angle Multiplexing Only
Approximate
Analysis
100 μm
Li and Psaltis
Page Size : 1000x1000 bits
Pixel Size : 3 micron
Index of Refraction : 2.2
Wavelength : 500 nm
Angle Multiplex:
10 to 20 degrees (inside)
Signal Beam on Axis
Bits/μm²
Thickness of Material (μm)
10⁰
10¹
10²
10³
10¹
10²
10³
10⁴
10⁵

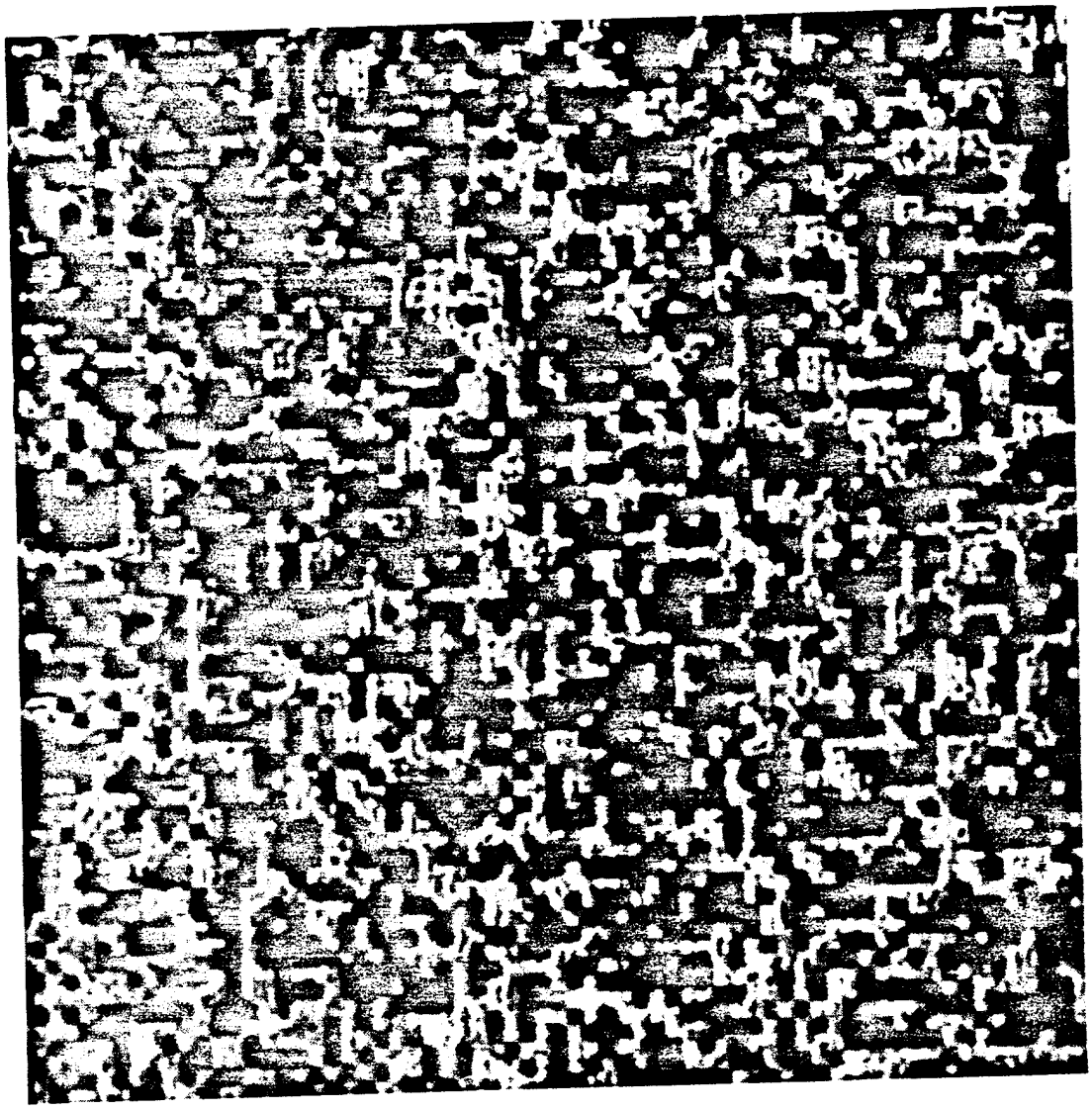

FIG 4

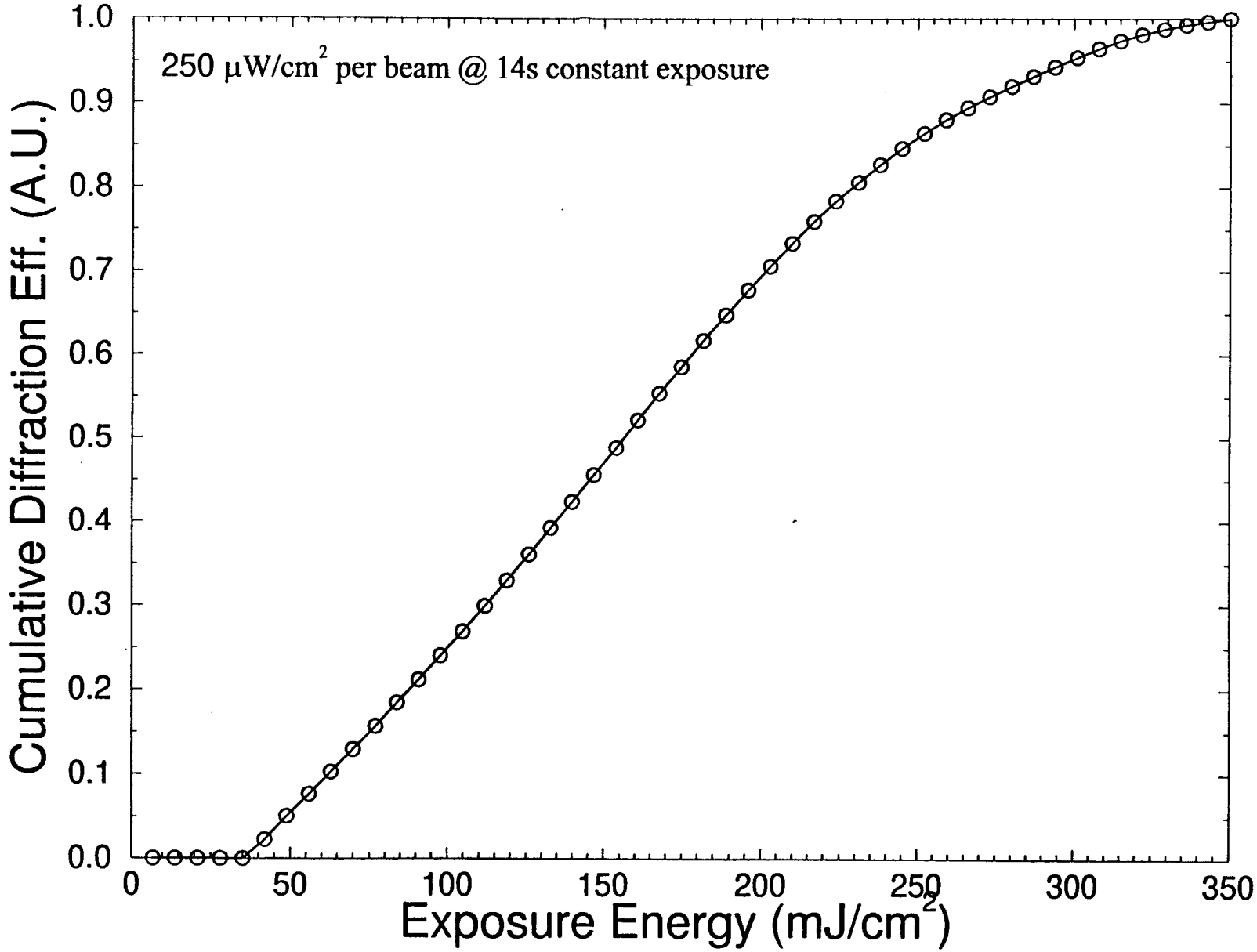
250 μW/cm² per beam @ 14s constant exposure
Cumulative Diffraction Eff. (A.U.)
Exposure Energy (mJ/cm²)
0.0
0.1
0.2
0.3
0.4
0.5
0.6
0.7
0.8
0.9
1.0
0
50
100
150
200
250
300
350

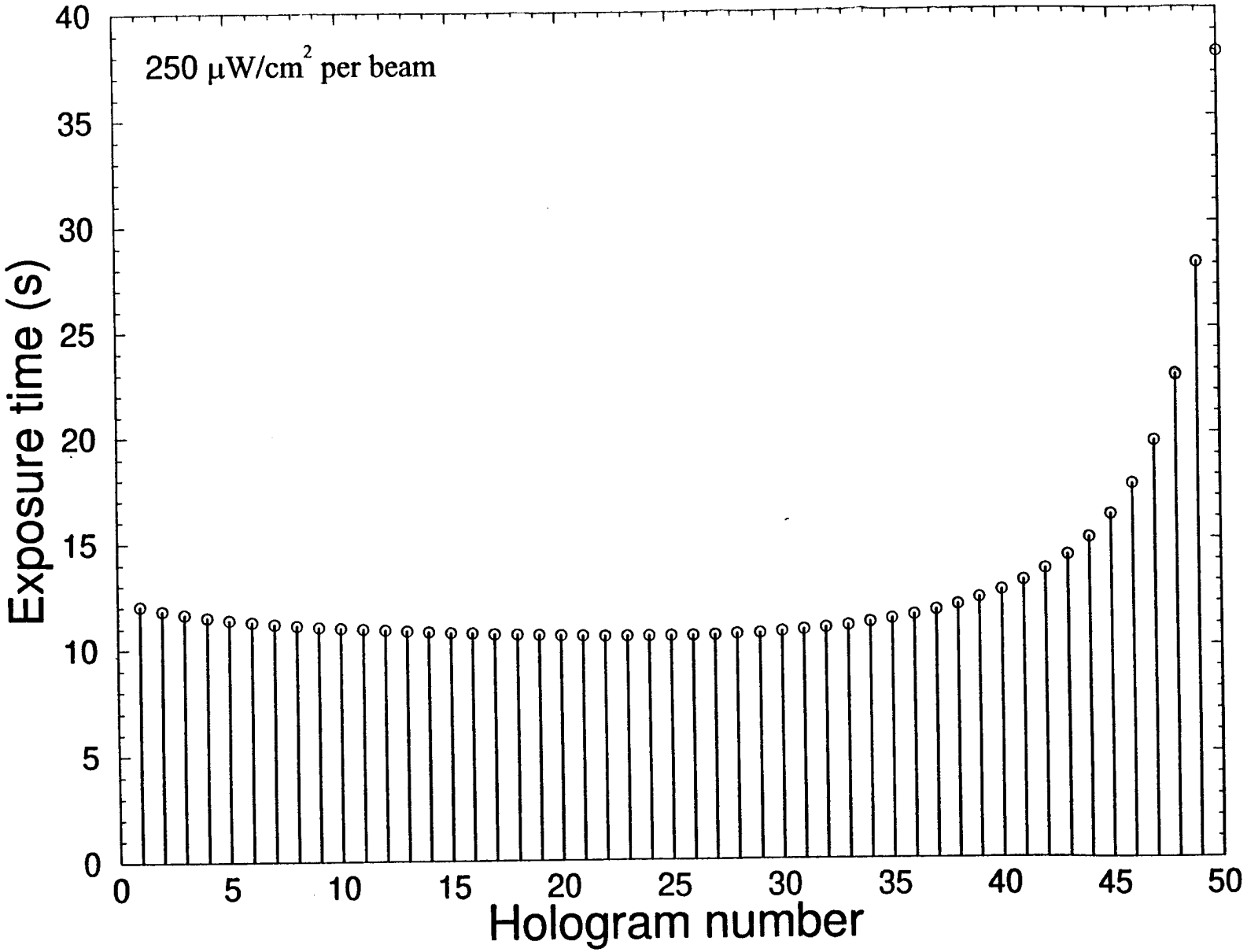
250 μW/cm² per beam
Exposure time (s)
Hologram number
0
5
10
15
20
25
30
35
40
45
50

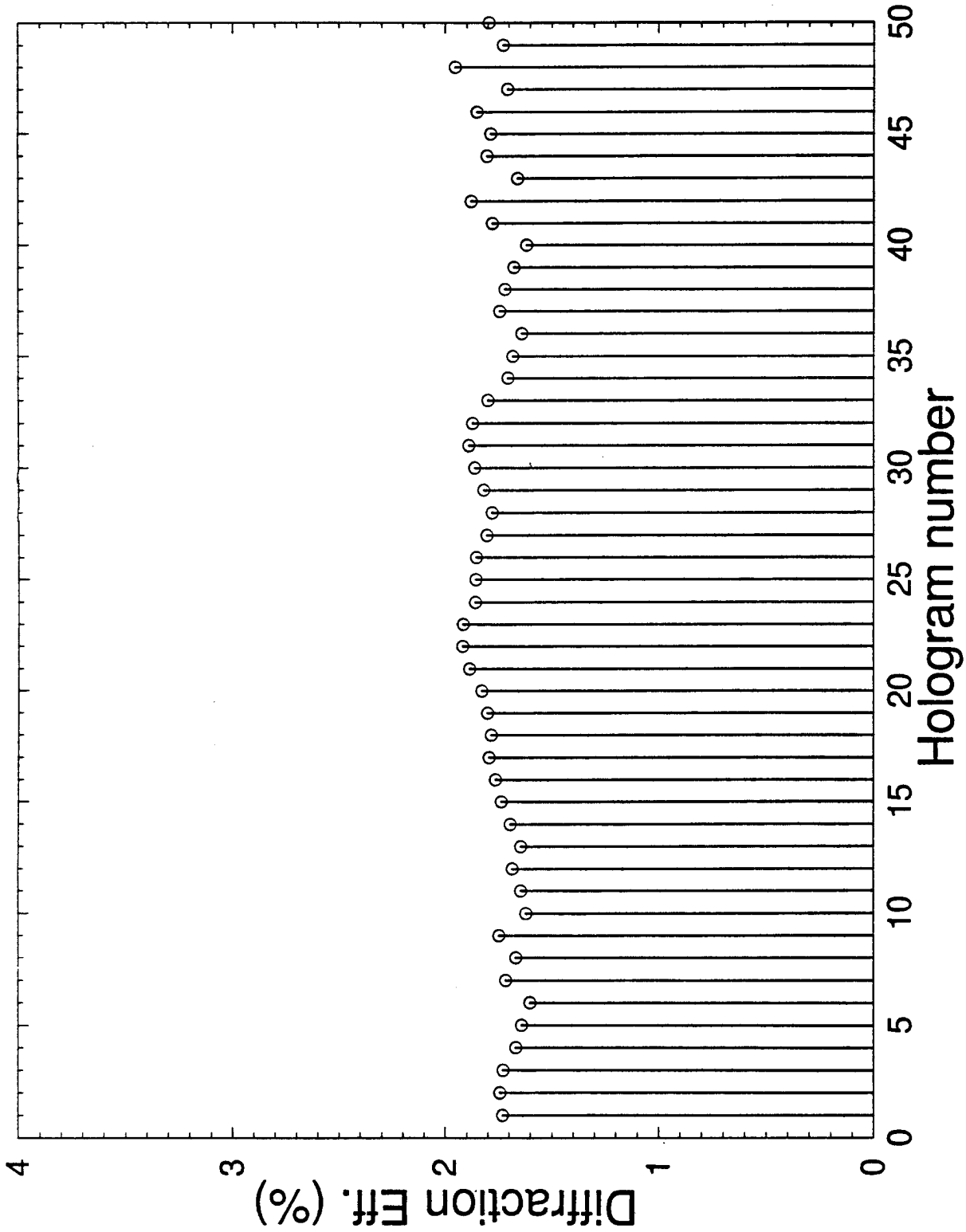

FIG 7 HDAOPA07.XGR

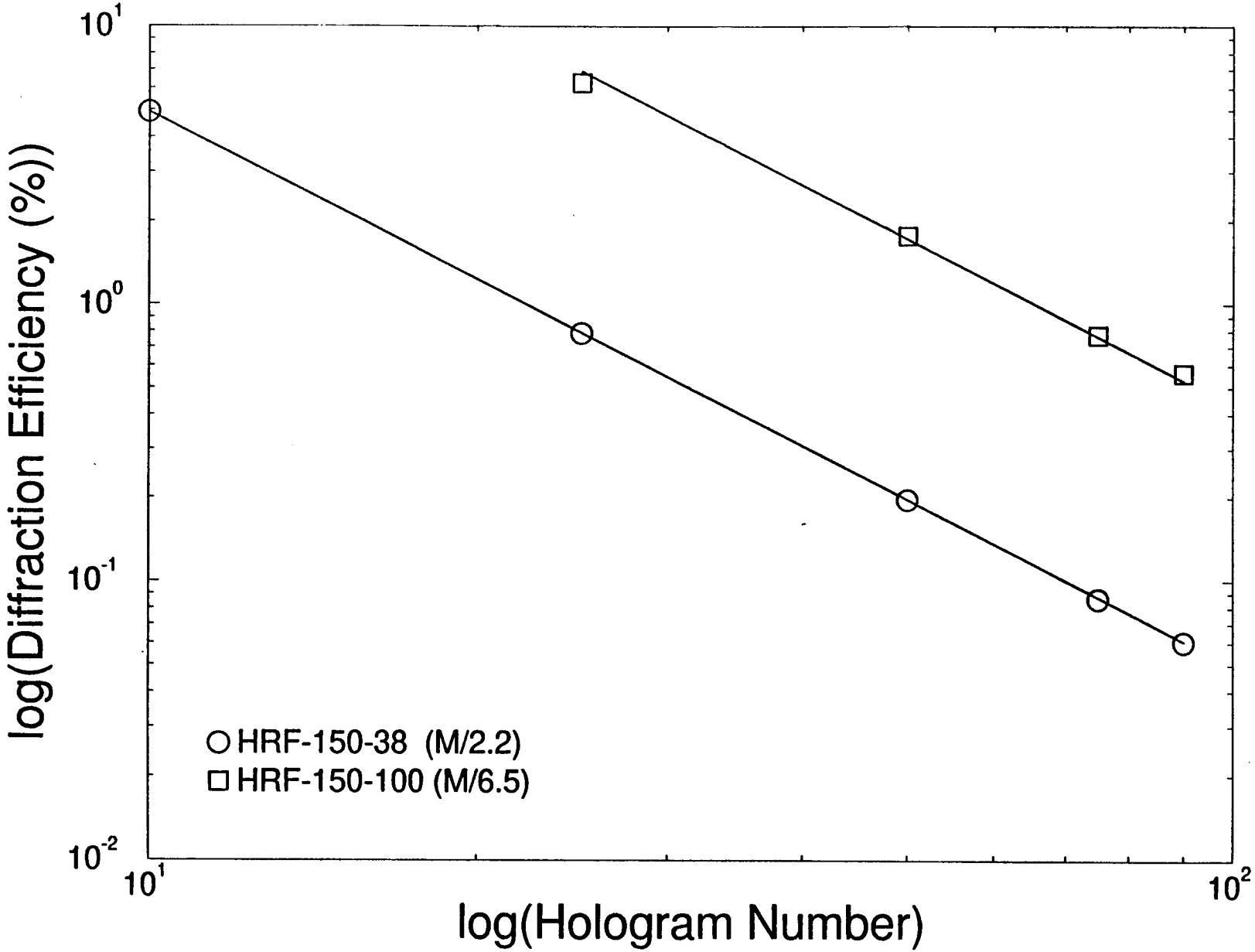
log(Diffraction Efficiency (%))
log(Hologram Number)
HRF-150-38 (M/2.2)
HRF-150-100 (M/6.5)
10^1
10^0
10^{-1}
10^{-2}
10^1
10^2

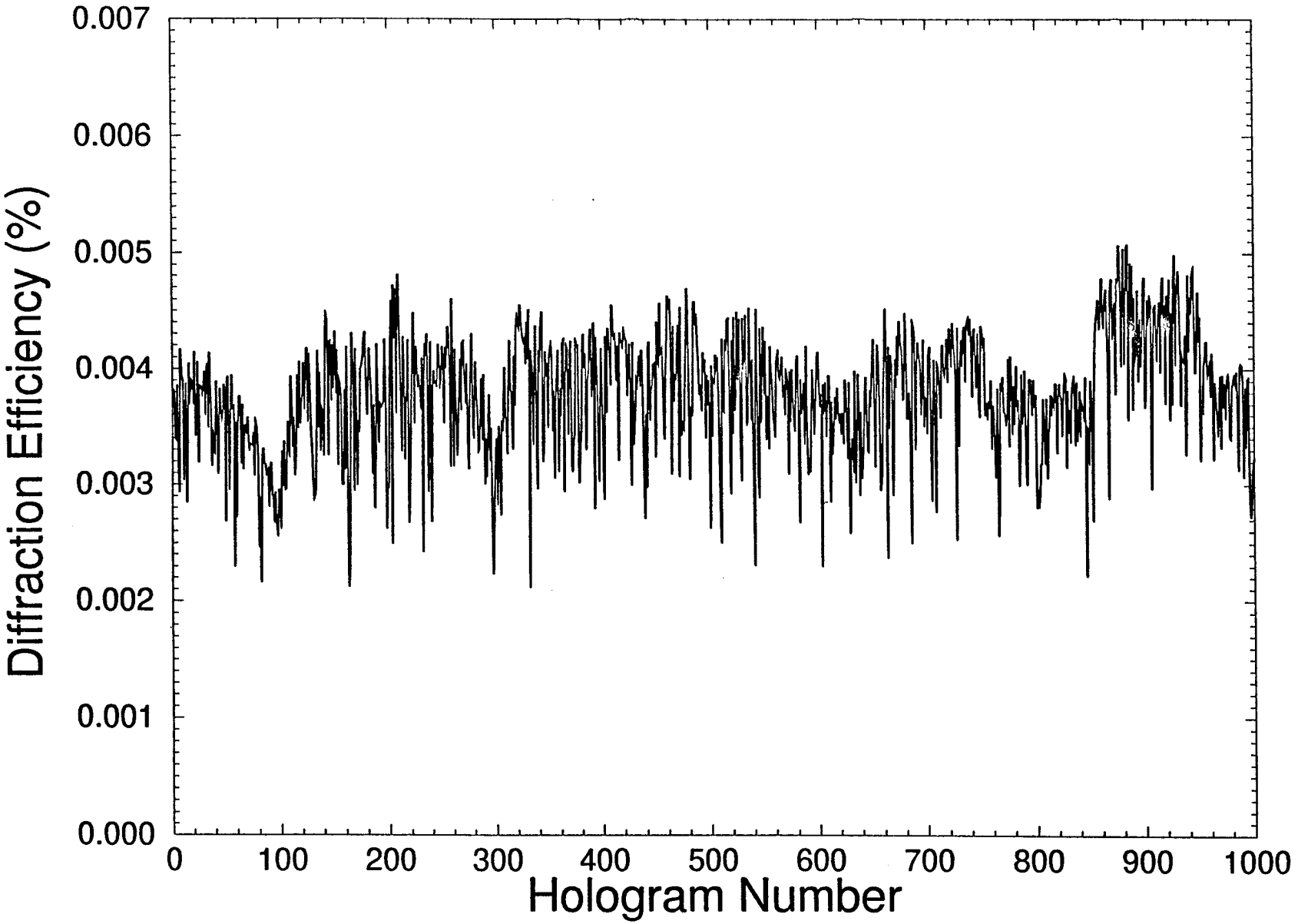
0.007
0.006
0.005
0.004
0.003
0.002
0.001
0.000
Diffraction Efficiency (%)
0
100
200
300
400
500
600
700
800
900
1000
Hologram Number

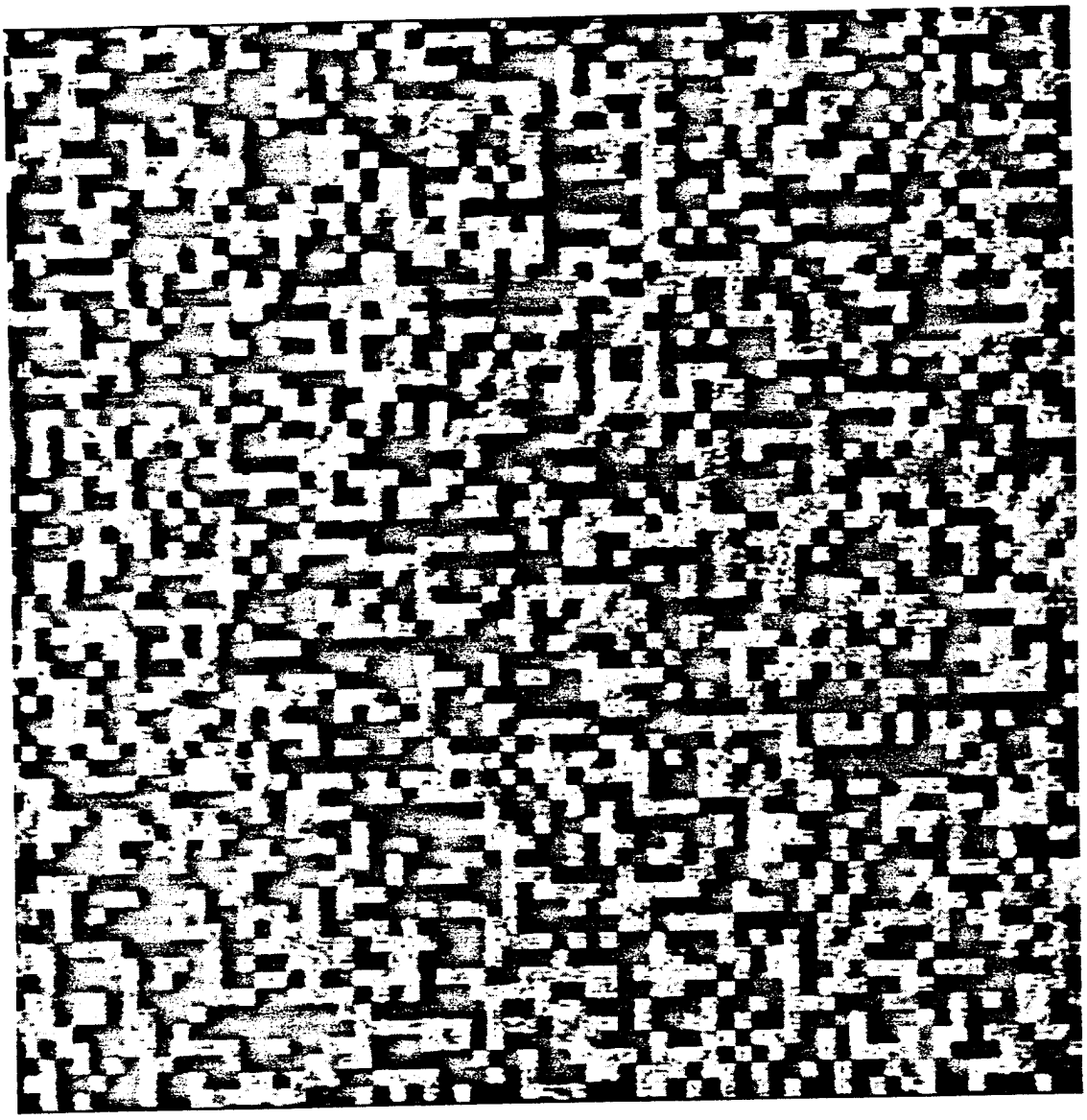

FIG 10

FIG 11 HDAGRAM X6A

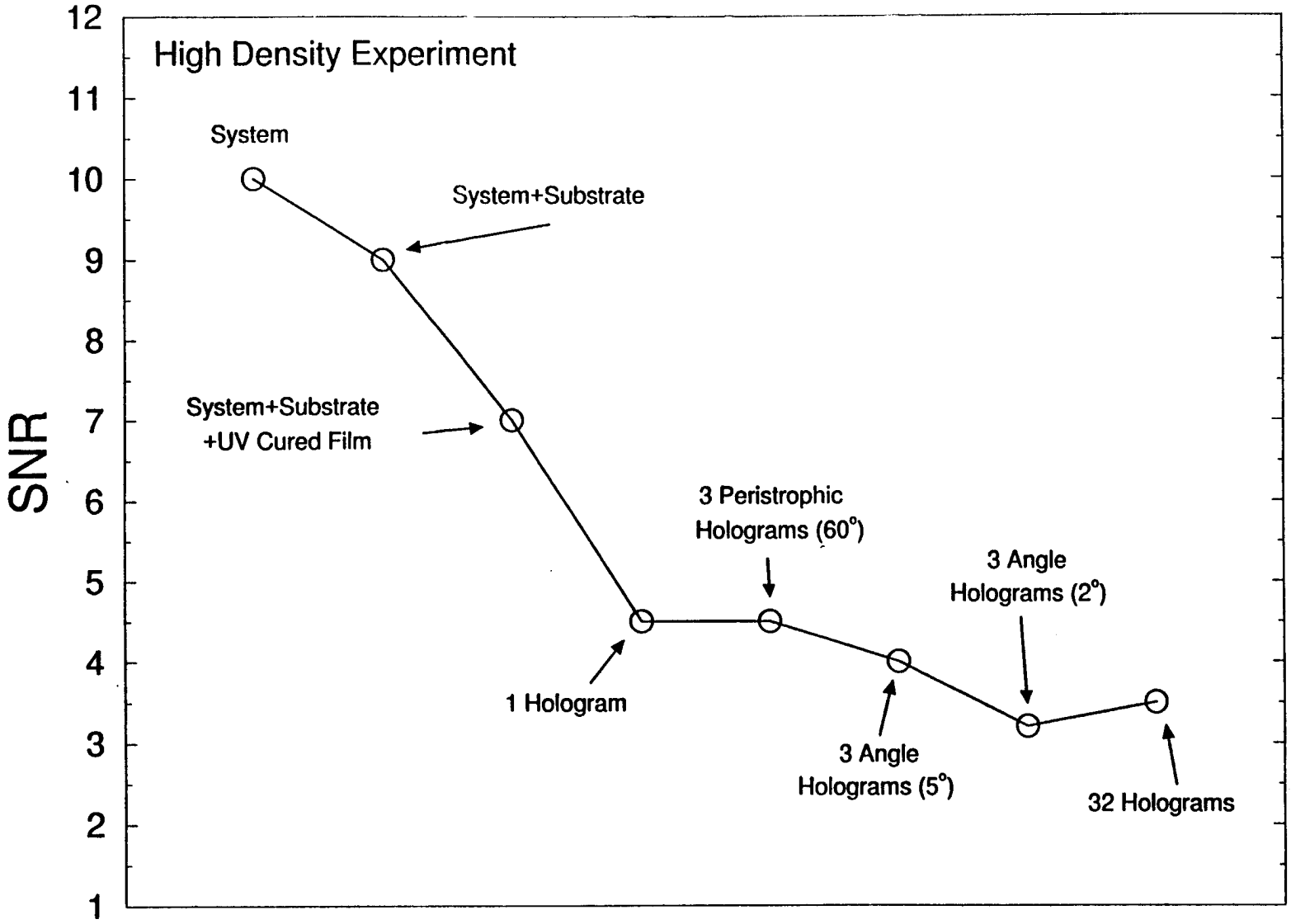
High Density Experiment
SNR
12
11
10
9
8
7
6
5
4
3
2
1
System
System+Substrate
System+Substrate
+UV Cured Film
1 Hologram
3 Peristrophic
Holograms (60°)
3 Angle
Holograms (5°)
3 Angle
Holograms (2°)
32 Holograms

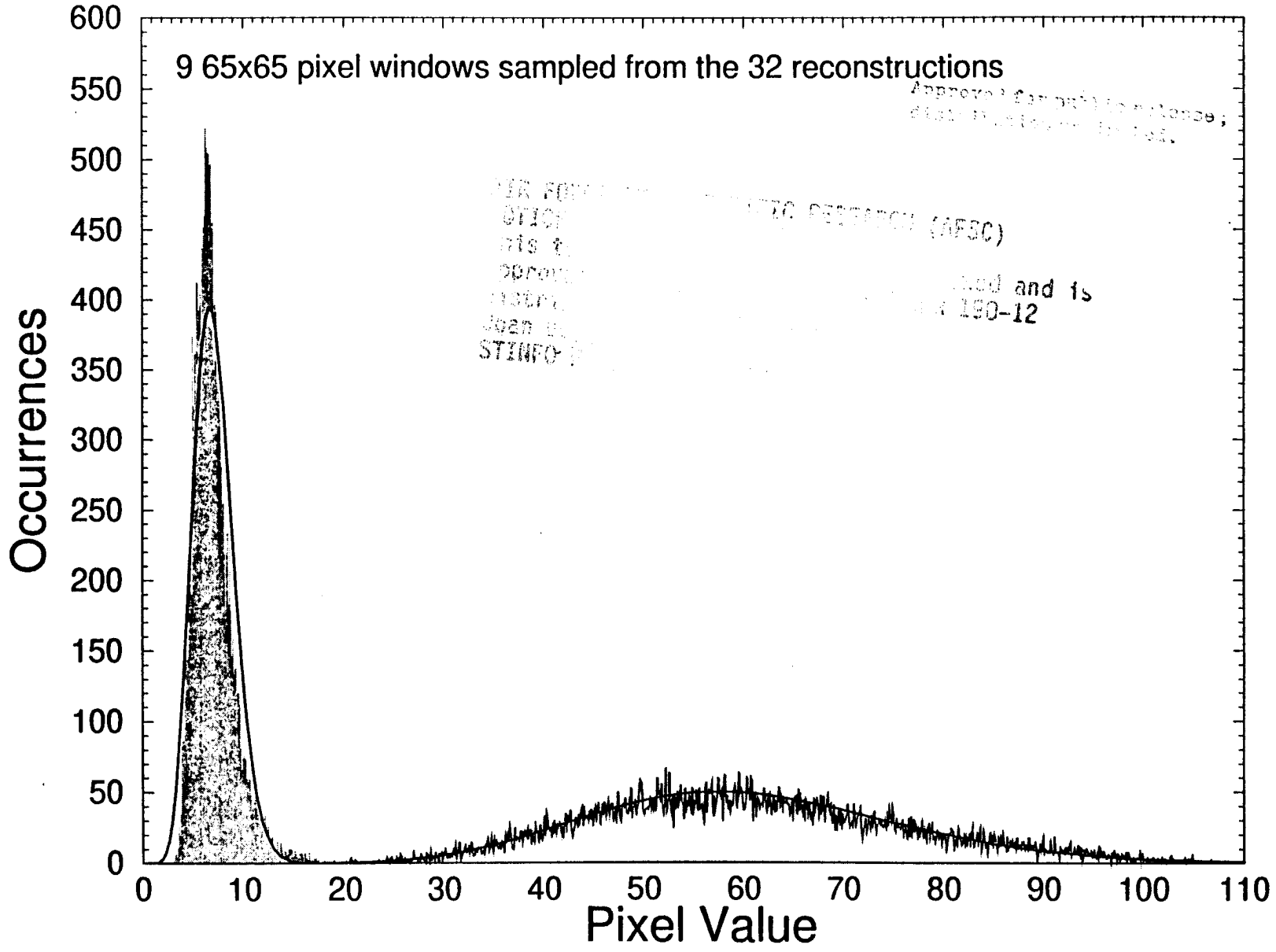

Fig 12 HDRDPA13.xgh